CrossMark

ORIGINAL PAPER

Variational Laws of Debris Flow Impact Force on the Check Dam Surface Based on Orthogonal Experiment Design

Xianbin Yu · Xiaoqing Chen

Abstract Debris flow impact force is an important factor for controlling structural damage, and it is the key factor for engineering design and risk assessment. Variation laws of debris flow impact force play an important role in preventing check dam impact damage and providing technology, data and support for check dam construction. Many influencing factors exist in debris flow impact force with different influencing magnitudes. The three main factors, i.e. the debris flow bulk density, the drainage channel slope and the upstream surface gradient of the check dam, were selected to be analyzed. The purpose of the study was to analyze the influencing degree of the three factors. Three levels were set for each factor and nine text schemes were established based on the theory of orthogonal experimental design. What is more, the related miniaturized flume experiment was carried out to measure impact force of debris flow. Finally, taking the impact force mean values of key point as the evaluation index, the flume experiment results were analyzed in detail by extreme difference analysis and variance analysis. Research results indicate: among the three factors, the drainage channel slope has the most significant influence, the upstream surface gradient of the check dam is in the second place and the debris flow slurry density is the third. The form of impact force mean with the maximum value: the drainage channel slope is 15°, the debris flow bulk density is 18.1 kN/m^3 and the upstream surface gradient of the check dam is 1:0.

Keywords Debris flow bulk density · Drainage channel slope · Upstream surface gradient of the check dam · Impact force · Orthogonal experiment design

1 Introduction

Debris flows endanger humans living in mountainous regions all over the world (Hübl et al. 2009). The design of structural mitigation measures, such as check dams and drainage channels, and the maintenance of infrastructures such as bridges require estimating the potential impact forces caused by debris flows (Scheidl et al. 2013). However, no entirely mechanistically and theoretically based impact model is currently sufficiently accurate and computable within periods common for design offices (Scheidl et al. 2013). The debris flow impact models used for engineering are mostly empirical or semi-empirical formulas. The impact force of debris flows

X. Yu (✉)
School of Civil Engineering and Architecture, Linyi University, Linyi 276005, China
e-mail: yuxianbin2006@126.com

X. Yu · X. Chen
Key Laboratory of Mountain Hazards and Surface Processes, Institute of Mountain Hazards and Environment, Chinese Academy of Sciences, Chengdu 610041, China

refers to a dynamic load produced by a moving debris flow process that contacts other objects; this major external force causes engineering damage to the debris flow areas of roads, bridges, and housing projects (Liu and Wei 1997; Chen et al. 2007). A debris flow is a typical solid–liquid two-phase flow. In the process of debris flow movement, the flow carries a wide particle size distribution of solid particles ranging from a few millimeters to tens of dollars. For this reason, it is difficult to use density, velocity, or deep mud to explain the differences in conditions of debris flow impacts (Hu et al. 2006). Moreover, because of the randomness of the impacting solid particles, the impact force of the debris flow is not the same under the same conditions at different locations (Iverson et al. 2010), further increasing the difficulty of studying the debris flow impact force. Over the years, determining the debris flow characteristics and impact load has been scientifically difficult, and this is still the weakness of debris flow dynamics (Wu et al. 1990). The main methods of obtaining debris flow impact force data include field measurements, model tests and numerical simulation. Measuring the impact of proto-typical debris flow fields is an important means of obtaining reliable data. Systematic observation of debris flow was conducted at Kamikamihori valley on the eastern slope of Mt. Yakedake in 1980, using a synthetic observation system equipped with many instruments and introducing various topographical surveys (Okuda and Okunishi 1980). Long-term observations were conducted using the natural advantages of Jiangjia Gully (Yunnan Province, China), where debris flows frequently occur. The time-history curves of the debris flow impact force were measured, and the eigenvalues of the debris flow impact force were analyzed (Zhang and Yuan 1985; Zhang 1993). As another example, debris flow impact piers were built in Jiangjia Gully (Yunnan Province, China). The time-history curves of the debris flow impact force were acquired using sensors and a microcomputer, and the debris flow impact load was taken into a sawtooth pulse, rectangular pulse and spike pulse (Wu et al. 1990). Field test devices were also established in Jiangjia Gully. Through the newly developed force sensors and data acquisition devices, the original impact signals at different positions of deep mud, long duration, and full waveform were measured and the real debris flow impact data were obtained by filtering the original signal (Hu et al. 2006, 2011). In situ

testing of debris flow was also conducted (König 2006; Wendeler et al. 2007). In addition, the impact force test of large-scale debris flow has been studied (DeNatale et al. 1999; Bugnion et al. 2012; Wendeler and Bugnion 2012). Using the large-scale debris flow test or monitoring stations to test the in situ observations of debris flow impact has the advantage of not needing to consider the scaling problem, and some important data can be obtained. However, the ability to control the boundary condition to acquire data is limited. For example, the occurrence frequency of a debris flow time is unknown, and the installation and operation of measuring equipment is the main drawback of natural debris flow observations. For large-scale debris flow tests, the expected volume of the material can lead to a too-costly measurement design; furthermore, the fluid and material parameters are often unpredictable (Scheidl et al. 2013).

Because of the above reasons, a large number of scholars have designed different physical models of debris flow impact tests based on the scaling consideration to study the impact of debris flow. Experimental research on the debris flow head impacting dams was conducted using flume tests: the composition of the impact force peak was analyzed, the calculation formula of the impact force of the debris flow head was established, and the vertical distribution of the debris flow impact force on the dam was determined (Wei 1996). Based on dynamic equilibrium analysis, the debris flow hydrodynamic pressure was analyzed using flume tests (Armanini and Scotton 1993). A larger-scale debris flow ditch test model was constructed, and a series of debris flow impact characteristics tests were conducted. The influences of the debris flow slurry viscosity, solid particle size and solid phase on the debris flow impact characteristics were studied, and some useful conclusions were obtained (Chen et al. 2010; He et al. 2013, 2014a, b). The debris flow velocity and impact characteristics were explored by flume tests and the relationship between the surface velocity of debris flow and the surface layer impact force was revealed (Yang et al. 2011). Model tests of the debris flow impact properties were performed, and the maximum impact of the debris flow was obtained by analyzing the experimental data (Scheidl et al. 2013). Debris flow impact tests were conducted using large flume tests. The original impact force signal obtained was subjected to wavelet denoising, and the calculation formula of the debris

flow liquid slurry impact, $p = 0.5\rho_f v^2$, was studied (Tang et al. 2013). The debris flow impact force was measured by the debris flow impact model test, and the debris flow impact speed ranged from 2 to 13 m/s (Bugnion et al. 2012). Impact force of viscous debris flow was measured by a miniaturized flume test and the impact force could be divided into three phases, i.e. the sudden strong impact of the debris flow, continuous dynamic pressure of the body and slight static pressure of the tail (Zeng 2014; Cui et al. 2015). The particle flow of the flume test was conducted first, and then the experiment was simulated by the discrete element software PFC 2D. Finally, the run-out distance and impact spectral characteristics of the particle flow were obtained (Valentino et al. 2008).

Based on previous studies, the three main factors of debris flow bulk density, drainage channel slope and upstream surface gradient of the check dam were selected as the main factors to carry out the orthogonal experiment design. The influence degree of the above three factors for debris flow impact force was obtained by range analysis and variance analysis. Research results can provide technical data and theoretical support for optimizing the design of check dams.

2 Debris Flow Impact Model

A corresponding adjustment coefficient of λ can be multiplied to consider the effect of stones in the debris flow. Taking the empty check dam as an example the impact pressure of the debris flow fluid can be expressed as:

$$\delta = \lambda \frac{\gamma_c}{g} v_c^2 \sin \alpha \qquad (1)$$

where δ is the overall impact pressure of the debris flow fluid (kPa); v_c is the section-averaged debris flow velocity (m/s); γ_c is the debris flow fluid density (kN/m³); g is the gravitational acceleration; α is the angle between the buildings and the stress surface of the debris flow impact pressure direction (°), where $sin\alpha$ is equal to 1 with vertical impact; and λ is the building shape coefficient, where λ is equal to 1.0 for circular buildings, 1.33 for rectangular buildings, and 1.47 for square buildings. For the check dam, λ of 1.47 is suitable for the water impact, and the value should increase when considering the impact of water and stones. When $D \leq 0.5$ m, λ is 1.47; when $D = 3$ m, λ

is 4; and when $D > 3$ m, λ is no greater than 8; the values for other cases can be obtained by linear interpolation (Jiang 2014).

3 Orthogonal Experimental Design

3.1 Orthogonal Testing Method

The orthogonal experimental design method is a highly efficient way capable of dealing with multifactor experiments and screening optimum levels by using the orthogonal design table, experimental results of which are studied by statistical method(Jiang 1985). Before making an orthogonal design table, reasonable and representative levels of all factors are determined at first according to theories or a few experiments. And then experiments represent all the level groups of the experimental factors are performed. Positive and negative factors and their impact degrees (ID) to the objective of production are revealed by calculating the experimental results, e.g. conversion and yield. The possible optimum level can be concluded according to the impact of the factors. At last, a confirmatory experiment is performed following the concluded optimum level (Tang and Feng 2002). Being compared with the general test method, orthogonal test method has two outstanding advantages. Firstly, in the arrangement, the number of experiments is reduced as far as possible. Secondly, on the basis of test data obtained by fewer times of experiments, the correct conclusion of practical guidance can be given, which is always a better result (Jia et al. 2014). For example, for an experiment with four factors and four levels of each factor, an orthogonal design table $L_{16}(4^4)$ could be used, and the experiment program only contains 16 level groups, reflecting the overall situation of the comprehensive experiment containing 256 level groups in all. Thus it is much easier to find out the optimum level group. (Jia et al. 2014, Ji et al. 2014).

3.2 Optimal Factors and Orthogonal Table

The first aim of the orthogonal experiments was to find the most important experimental factor on the performance of debris flow impact force. The second aim was to detect the optimum operational parameters to obtain the minimum mean value of impact force. Before arranging the orthogonal experimental matrix,

the reasonable and condensed levels of each experimental factor should be chosen.

According to the above impact pressure expression 1 and preliminary experimental experiences, these three factors shown as follows: L (drainage channel slope), M (upstream surface gradient of the check dam), N (debris flow bulk density) are chosen as the experimental factors, which are shown in Table 1. Each factor includes three levels as: L: 9°, 12° and 15°; M: 1:0, 1:0.15, and 1:0.3; N: 14.2, 18.1, and 19.5 kN/m^3.

There are three experimental factors and three levels for each factor, choosing an orthogonal table is the other important work. Orthogonal tables play an important role in the arrangement of the whole test process and results, which are considered to be the most important part of the whole orthogonal experiment design. As the factors and their levels are shown in the Table 1, an orthogonal table noted as $L_9(3^4)$ (shown in Table 2) can be chosen as the experimental scheme to arrange the experiments. "9" stands for the orthogonal table rows, namely the maximum number of tests and each row of orthogonal table represents a run with a specific set of levels to be tested. "4" means the orthogonal array that is the maximum number of factors can be arranged. Because this study has only three factors, more than one column can be used to arrange the error term (e). "3" represents the level of the factors. During the test, the experimental order was random to avoid possible subjective bias.

3.3 Analytical Methods of Experiment Results

Impact force mean values of debris flow on the upstream surface of the check dam are taken as the test index. The points, which are on the dam abutment or overflow section of the check dam, are selected as the representatives to be studied, rather than only for a point or some points at a position. Only in this way,

Table 1 Factors of the orthogonal table and their levels

Levels	Orthogonal factors		
	L /°	M	N /kNm^{-3}
1	9	1:0	14.2
2	12	1:0.15	18.1
3	15	1:0.30	19.5

Table 2 Schemes of orthogonal test design of impact force

No.	e	L /°	M	N /kNm^{-3}
1	1	9	1:0	14.2
2	1	12	1:0.15	18.1
3	1	15	1:0.30	19.5
4	2	9	1:0.15	19.5
5	2	12	1:0.30	18.1
6	2	15	1:0	14.2
7	3	9	1:0.30	18.1
8	3	12	1:0	19.5
9	3	15	1:0.15	14.2

can impact force of debris flow of the whole dam upstream surface be understood comprehensively. A relatively more reasonable conclusion can be obtained by the comprehensive analysis of impact force of the multiple representative points. Figures 1 and 2 show the location diagram of representative points. As the experimental times have been reduced greatly, the method to process the orthogonal experimental data was very important. The range analysis and variance analysis are usually used to detect the most sensitive factor influencing the target index, and verify the distinctiveness in the researches. In this study, the range analysis and variance analysis are selected to
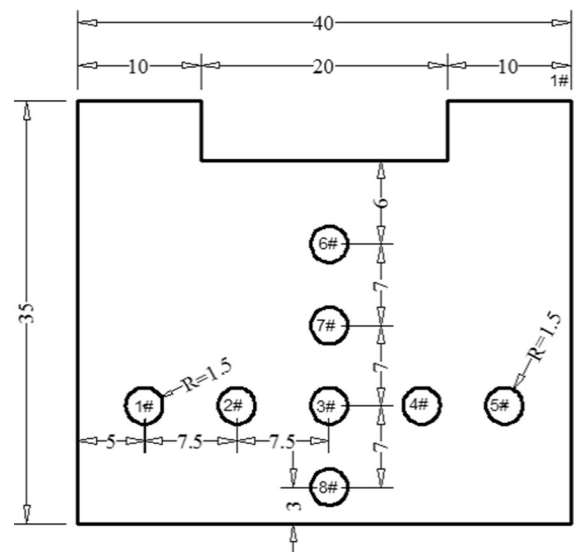
Fig. 1 Plane arrangement of investigated points of the check dam

Fig. 2 The pressure sensor layout

deal with the test results, and the sensitivity of different factors is studied.

3.3.1 Range Analysis

The range analysis is an image visual analysis method, which is simple, concise, and easy to understand and operate. Range analysis, R method for short, normally involves two steps of calculation and judgment. Flow diagram of R method procedures is shown in the Fig. 3.

In this study, the range analysis is employed to discriminate the comparative significance of each factor, which was defined as the difference between

the maximum and minimum value of $\overline{K_{ij}}$ the j-th factor, noted as $\overline{R_j}$

$$\overline{R_j} = \max\left(\overline{K_{1j}}, \overline{K_{2j}}, \cdots \overline{K_{ij}}\right) - \min\left(\overline{K_{1j}}, \overline{K_{2j}}, \cdots \overline{K_{ij}}\right) \tag{2}$$

where $\overline{K_{ij}}$ is the average targeting value of each experimental factor at the same level in the orthogonal experiments, which was used to determine the optimal level and the optimal combination of factors. $\overline{K_{ij}}$ can be expressed as:

$$\overline{K_{ij}} = \frac{K_{ij}}{n} \tag{3}$$

$$K_{ij} = \sum_{k=1}^{p_1} Y_{ijk} \tag{4}$$

where the Arabic numerals i ($i = 1, 2, 3$) are the level number and j ($j = L, M, N$) donated a certain factor. K_{ij} is the sum of the targeting indexes of all levels in each factor j; n is the total levels of the corresponding factor. Y_{ijk} is the k-th test result index value, with the j-th factor and the i-th level. A larger $\overline{R_j}$ means a greater importance of the factor.

3.3.2 Analysis of Variance

In the test process, because of the existence of the subjective and objective factors, there is a certain error between the experimental results and the real results. Range analysis shows the order of the variables
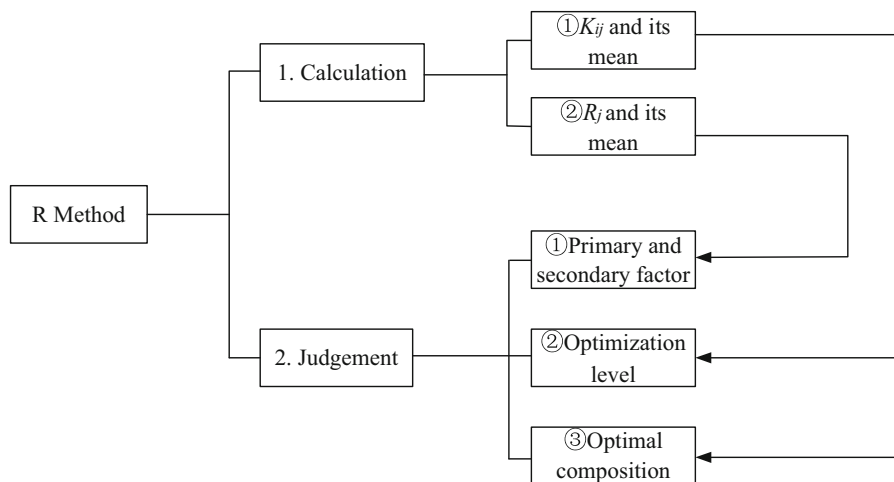
Fig. 3 Flow diagram of R method procedures

influencing on the target by intuition. However, it cannot distinguish whether the undulation of each factor level is caused by the varying levels or by the experimental errors. Moreover, it cannot provide a standard to estimate whether the influence of variable is noticeable. In order to overcome this limitation, a variance analysis is necessary to obtain the magnitudes of the factor affecting the targeting index.

The variance analysis first divided the total fluctuation into two parts: the fluctuation coming from the experimental conditions and generated from the experimental error; and then the two part fluctuation are compared with each other by statistics analysis; finally, the conclusion can be obtained according to the comparative results. As the F value of each factor can be used to indicate the ratio of the sum of the square of each factor's mean deviation to that of the experimental error. Therefore, the F-test is employed to analyze the experimental data, and the F value is used to indicate the degree of the factor's influencing, which can be calculated by the following formulas (Jia et al. 2014).

$$S_{sum} = \sum_{i=1}^{n} \sum_{k=1}^{p_1} \left(Y_{ijk}\right)^2 - \frac{T^2}{p_0} \tag{5}$$

$$S_j = \frac{\sum_{i=1}^{n} \left(K_{ij}\right)^2}{p_1} - \frac{T^2}{p_0} \tag{6}$$

$$S_e = S_{sum} - \sum_{j=1}^{m} S_j \tag{7}$$

$$T = \sum_{i=1}^{n} \sum_{k=1}^{p_1} Y_{ijk} \tag{8}$$

where S_{sum} stands for total differences; S_j reflects the differences of experimental results caused by the change in every level of factor j, which shows the influence of factor j on the experimental results; S_e reflects the differences of experimental results caused the error; m is the number of the factors; p_1 stand for test times with the j-th factor and the i-th level; p_0 stand for the total test times; T stands for the sum of test indexes; Other symbols are the same as the above.

Given a specific test level, ζ (degree of confidence), the critical value, $F_\zeta(f_j, f_e)$ can be found in the F distribution table. The F values of each factor are compared with $F_\zeta(f_j, f_e)$. A larger F value of the factor means a more significant effect for test index. F can be expressed as:

$$F = \frac{S_j/f_j}{S_e/f_e} \tag{9}$$

where f_j represents degree of freedom of each factor; f_e stands for degree of freedom of test error; and other symbols are the same as the above. f_j and f_e can be expressed as:
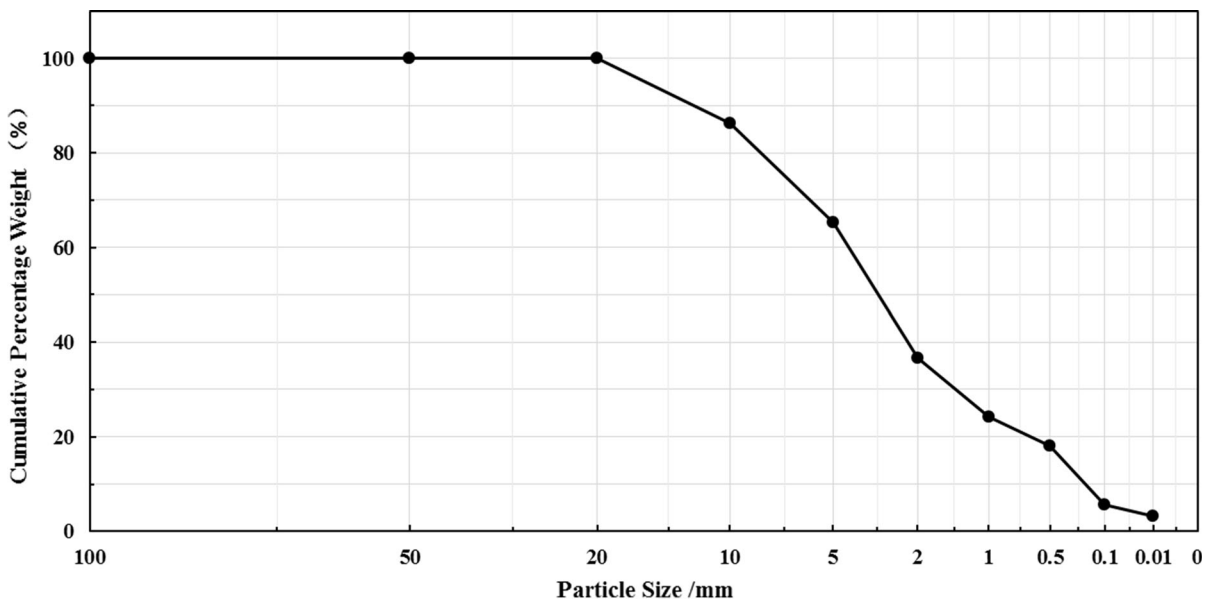

Fig. 4 Gradation/particle size distribution of the debris flow in the test model

$$\begin{cases} f_e = f_T - \sum f_j \\ f_j = n - 1 \\ f_T = p_0 - 1 \end{cases} \qquad (10)$$

4 Debris Flow Impact Force on the Surface of Check Dams

4.1 Experimental Setup

4.1.1 Experimental Materials

The experiments were conducted at the Dongchuan Debris Flow Observation and Research Station at the Chinese Academy of Sciences. An original sample of the debris flow materials from the Jiangjia Gully was used in the experiment because debris flows from this area are typical of the flows that were found in most of the mountainous regions in China. The particle diameter of the test model materials is limited by the use of a 20 × 20 mm steel mesh, which rejects gravel soil particles with diameters >20 mm. The particle size distribution of the soil sample is shown in Fig. 4. The median particle size of the soil sample is 2.5 mm,

and the contents of particles <1 mm and <0.1 mm are approximately 24.3 and 5.6%, respectively.

4.1.2 Experimental Model

The test model mainly consists of the following four components: a drainage channel, check dam, tailing pool, and hopper. The experiments were conducted in an 8-m-long open-water channel with a rectangular cross section of 0.4 × 0.5 m (width × height). All of the sidewalls in the test section were reinforced glass, the bottom slab was steel plate, and the check dam was steel plate. The upper portion of the dam section was 0.2 m, the underside was 0.34 m, the dam height was 0.35 m, and the dam length was 0.4 m. The slope of the front of the dam was 1:0.3, while the slope behind the dam was 1:0; the width and height of the overflow mouth were 0.2 and 0.05 m, respectively. Figure 5 shows the three-dimensional diagram and panorama of the test model.

4.1.3 Measurement System

The measuring device consisted of the following three components: eight modified pressure sensors, a high-

Fig. 5 Three-dimensional diagram and panorama of the test model
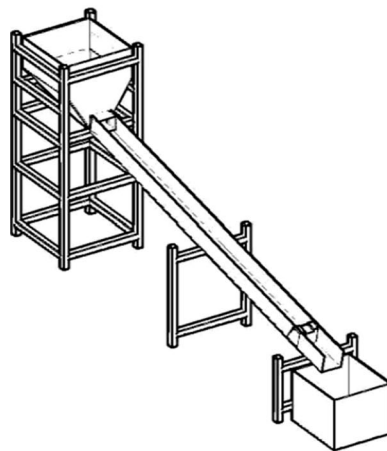
Table 3 Technical parameters of the pressure sensors

Model	Precision (%)	Measurement range (MPa)	Temperature range (°C)	Power supply (DC) (V)	Output signal of the transmitter (V)	Physical dimensions (mm)
JNBP-6	0.1	0.6	−30–70	20	0–5	R = 15, h = 30

speed continuous data acquisition instrument, and data collection procedures.

4.1.3.1 Pressure Sensors Eight pressure sensors, which were used to measure the debris flow fluid impact, were arranged vertically and horizontally along the check dam upstream face. The two-dimensional layout schematic of the pressure sensors and the numbers of the eight sensors are shown in Fig. 1. Figure 2 shows the arrangement of the pressure sensors along the check dam upstream face. The pressure sensors are piezoresistive sensors, and the relevant parameters of the pressure sensors are shown in Table 3.

4.1.3.2 Data Acquisition Instrument The data acquisition instrument is the high-speed continuous collection instrument. The relevant model and characteristic parameters are shown in Table 4.

4.1.4 Data Collection Procedures and Binary Data Export Tool

A denoising method based on wavelet transformation was used in the software components; this method has better filtering in the sharp white noise signal of the time domain signals acquired by the pressure sensors. The acquisition frequency, acquisition time and other physical quantities can be set up in the master interface of the data collection procedures. The acquisition frequency of the data collection procedures can range from 0.1 to 2200 Hz. The acquisition frequency in the experiment was set to 1000 Hz according to the research needs. Due to the large amount of data and to improve the collection efficiency of the data collection procedures, the data collected by the data acquisition program were automatically saved as binary data in a .bat file format; the binary data were then converted to decimal data with an .xlsx file format via an export tool.

4.2 Analysis of Experimental Results

According to orthogonal test design shown in the Table 2, nine sets of numerical simulation are carried out, and finally, the required data are extracted. The specific statistical data of mean values of debris flow impact force of investigated points are shown in Table 5.

Table 5 shows that, among the nine test cases, mean values of impact force in the position of 8# point is the maximum value, while the position of 6# point has the

Table 4 Technical parameters of the data acquisition instrument

Model	Precision (%)	Analysis bandwidth (kH)	Power supply (DC) (V)	Output signal		Physical dimension (mm)
JN-BSQ	0.03	10	AC220	Digital signal		220
Number of channels	Sampling method	Sampling frequency (kHz)	A/D converter	Operating temperature (°C)		Noise (dB)
8	Synchronous sampling	20	16's column	−20–70		85

Table 5 Mean values of debris flow impact force of investigated points (Unit: kPa)

No.	1#	2#	3#	4#	5#	6#	7#	8#
1	5.49	6.48	6.69	6.38	5.40	1.24	2.01	7.23
2	10.46	11.98	11.76	11.56	10.56	2.68	4.21	12.36
3	11.66	12.35	12.46	12.12	11.59	3.21	5.12	13.56
4	5.89	6.63	6.73	7.00	6.12	1.11	2.68	9.12
5	10.40	11.01	11.31	10.96	10.24	2.56	4.01	12.04
6	12.01	11.99	12.31	11.95	12.12	3.89	4.53	13.12
7	6.31	6.95	7.07	7.12	6.24	1.49	2.96	9.21
8	10.75	11.66	11.86	11.76	10.28	2.31	4.28	12.86
9	11.68	11.77	11.89	11.56	11.6	3.68	4.41	13.02

minimum value. The impact force mean values of the overflow section are greater than that of the abutment position of the check dam. The mean values of impact force decrease as the check dam's height increases.

4.3 Range Analysis

Using the range analysis method introduced in Sect. 3.3.1, the range analysis of the impact force mean values of the investigated points is carried out and the range analysis results are given in Table 6. The range value (R_j) expresses the significance of the influence of the factors. The factor with larger R_j has a great effect on debris flow impact force. Trend chart of mean values of impact force and factor levels is shown in the Fig. 5.

Table 6 indicates that, among the eight test index, number of times of the most significant factor is: eight times with L, zero time with M, zero time with N; number of times of the most secondary factor is: zero time with L, eight time with M, zero time with N. According to the R_j value of each factor, among the eight test index, the order of the factors' impact is as follows: the drainage channel slope > debris flow bulk density > the upstream surface gradient of the check dam. The R_L is the largest among all these ranges, implying that the drainage channel slope is the most significant factor influencing on the debris flow impact force. The mean values of impact force debris flow of the eight key points are the largest under the working condition of $L_3M_1N_3$.

Table 6 Extreme difference analysis of impact force mean values

Test index	Mean value of impact force /kPa (1#)			Mean value of impact force /kPa (2#)			Mean value of impact force /kPa (3#)			Mean value of impact force /kPa (4#)		
	L	M	N	L	M	N	L	M	N	L	M	N
K_{1j}	5.90	9.42	9.19	6.69	10.04	9.75	6.83	10.29	9.96	6.83	10.03	9.63
K_{2j}	10.54	9.34	9.59	11.55	10.13	10.31	11.64	10.13	10.38	11.43	10.04	10.21
K_{3j}	11.78	9.46	9.43	12.04	10.10	10.21	12.22	10.28	10.35	11.88	10.07	10.29
$\bar{K}_{1j}$	1.97	3.14	3.06	2.23	3.35	3.25	2.28	3.43	3.32	2.28	3.34	3.21
$\bar{K}_{2j}$	3.51	3.11	3.20	3.85	3.38	3.44	3.88	3.38	3.46	3.81	3.35	3.40
$\bar{K}_{3j}$	3.93	3.15	3.14	4.01	3.37	3.40	4.07	3.43	3.45	3.96	3.36	3.43
R	5.89	0.11	0.40	5.35	0.08	0.55	5.39	0.16	0.42	2.28	0.04	0.66
$\bar{R}$	1.96	0.04	0.13	1.78	0.03	0.18	1.80	0.05	0.14	0.76	0.01	0.22
Primary and secondary levels	1 2 3	2 1 3	1 3 2	1 2 3	1 3 2	1 3 2	1 2 3	2 3 1	1 3 2	1 2 3	1 2 3	1 2 3
Primary and secondary factors	$L\,N\,M$			$L\,N\,M$			$L\,N\,M$			$L\,N\,M$		
Test index	Mean value of impact force /kPa (5#)			Mean value of impact force /kPa (6#)			Mean value of impact force /kPa (7#)			Mean value of impact force /kPa (8#)		
	L	M	N	L	M	N	L	M	N	L	M	N
K_{1j}	5.92	9.27	9.08	1.28	2.48	2.49	2.55	3.61	3.48	7.52	11.07	10.76
K_{2j}	10.36	9.43	9.64	2.52	2.49	2.69	4.17	3.77	3.90	12.42	11.50	10.56
K_{3j}	11.77	9.36	9.33	3.60	2.43	2.22	4.69	4.03	4.03	13.23	10.60	11.85
$\bar{K}_{1j}$	1.97	3.09	3.03	0.43	0.83	0.83	0.85	1.20	1.16	2.51	3.69	3.59
$\bar{K}_{2j}$	3.45	3.14	3.21	0.84	0.83	0.90	1.39	1.26	1.30	4.14	3.83	3.52
$\bar{K}_{3j}$	3.92	3.12	3.11	1.20	0.81	0.74	1.56	1.34	1.34	4.41	3.53	3.95
R	5.85	0.16	0.56	2.32	0.06	0.47	2.14	0.42	0.55	5.71	0.90	1.28
$\bar{R}$	1.95	0.05	0.19	0.77	0.02	0.16	0.71	0.14	0.18	1.90	0.30	0.43
Primary and secondary levels	1 2 3	1 3 2	1 3 2	1 2 3	1 2 3	1 2 3	1 2 3	1 2 3	1 2 3	1 2 3	3 1 2	2 1 3
Primary and secondary factors	$L\,N\,M$			$L\,N\,M$			$L\,N\,M$			$L\,N\,M$		

Figure 6 shows the average value of each factor. It should be mentioned that the graph is only used to show the trends of each factor, not to predict other levels untested experimentally in this study. The statistical parameter $\overline{K_{ij}}$ increases with the increase in the level values of the drainage channel slope, decreases in a small scale with the increase in the level values of the upstream surface gradient of the check dam except for the key point of 7# and 8#, and increases and then decreases with the increase in the level value of debris flow bulk density.

4.4 Analysis of Variance

Using the analysis of variance method introduced in Sect. 2.3.2, the range analysis of the impact force mean values of the investigated points is carried out and the variance analysis results are given in Table 7. $F_{0.05}$ (2, 2) = 19.0, $F_{0.1}$ (2, 2) = 9.0, and $F_{0.25}$ (2, 2) = 3.0 have been queried by the F distribution table and listed into the Table 7.

As shown in Table 7, eight times with L, zero time with M and N meet the expression of $F > F_{0.05}$ (2, 2) = 19.0; eight times with L, zero time with M and three times with N meet the expression of $F > F_{0.1}$ (2, 2) = 9.0 and eight times with L, one time with M and

six times with N meet the expression of $F > F_{0.25}$ (2, 2) = 3.0. The above results indicate the order of the effect of the three factors is as follows: the drainage channel slope > debris flow bulk density > the upstream surface gradient of the check dam, which is in accord with the results of range analysis.

5 Conclusions

In this study, design of orthogonal test first carried out to determine the number of test groups and obtain the orthogonal table. Secondly, miniaturized flume experiments are carried out to measure impact force of debris flow according to the orthogonal table and the test date are obtained and dealt with. At last, the range and variance analysis of the test date are carried out. The main points could be concluded as the following:

1. The range analysis and variance analysis of the test results show that indicate the order of the effect of the three factors is as follows: the drainage channel slope > debris flow bulk density > the upstream surface gradient of the check dam, which indicates the drainage channel slope is the most significant factor.
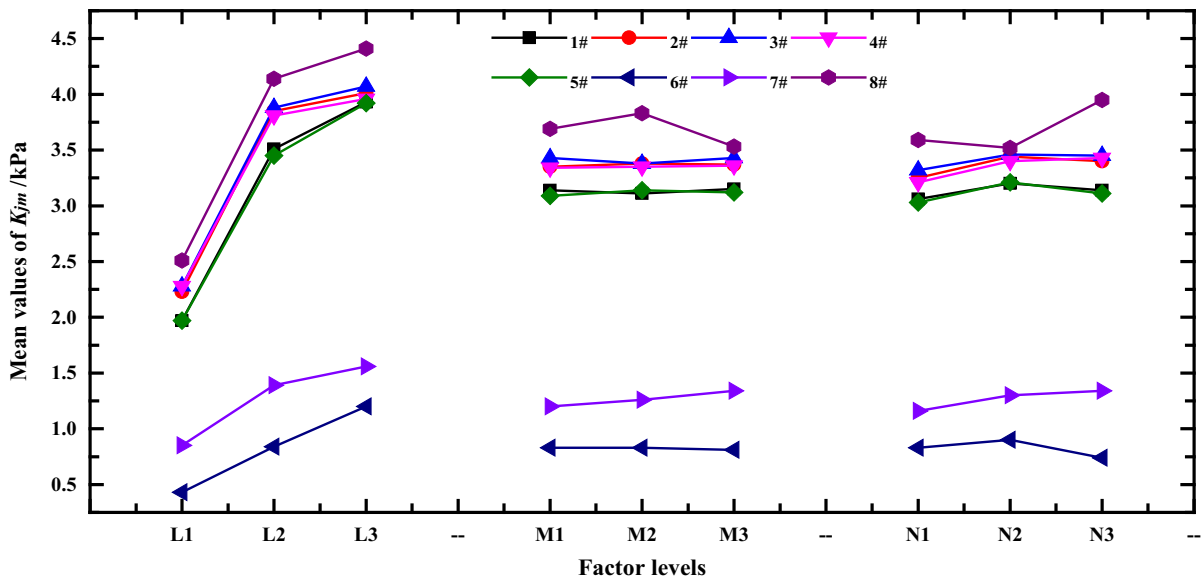

Fig. 6 Tendency of impact force mean values and influence level of the factor

Table 7 Variance analysis of impact force mean values

Test index	Variance source	Sum of squares of variation	Degree of freedom	Average variation	Values of F	Critical value of F		
						$\zeta = 0.05$	$\zeta = 0.10$	$\zeta = 0.25$
Mean values of impact force (1#)	L	57.737	2	28.869	267.301	19.0	9.0	3.0
	M	0.020	2	0.01	0.093	19.0	9.0	3.0
	N	0.247	2	0.124	1.144	19.0	9.0	3.0
	e	0.216	2	0.108		19.0	9.0	3.0
Mean values of impact force (2#)	L	52.511	2	26.256	220.634	19.0	9.0	3.0
	M	0.011	2	0.0055	0.046	19.0	9.0	3.0
	N	0.526	2	0.263	2.210	19.0	9.0	3.0
	e	0.238	2	0.119		19.0	9.0	3.0
Mean values of impact force (3#)	L	52.553	2	26.277	875.883	19.0	9.0	3.0
	M	0.049	2	0.025	0.817	19.0	9.0	3.0
	N	0.324	2	0.162	5.40	19.0	9.0	3.0
	e	0.06	2	0.03		19.0	9.0	3.0
Mean values of impact force (4#)	L	46.736	2	23.368	934.720	19.0	9.0	3.0
	M	0.002	2	0.001	0.040	19.0	9.0	3.0
	N	0.775	2	0.388	15.50	19.0	9.0	3.0
	e	0.050	2	0.025		19.0	9.0	3.0
Mean values of impact force (5#)	L	55.924	2	27.962	380.435	19.0	9.0	3.0
	M	0.039	2	0.020	0.265	19.0	9.0	3.0
	N	0.472	2	0.236	3.211	19.0	9.0	3.0
	e	0.147	2	0.074		19.0	9.0	3.0
Mean values of impact force (6#)	L	8.108	2	4.054	270.267	19.0	9.0	3.0
	M	0.006	2	0.003	0.200	19.0	9.0	3.0
	N	0.330	2	0.165	11.000	19.0	9.0	3.0
	e	0.030	2	0.015		19.0	9.0	3.0
Mean values of impact force (7#)	L	7.449	2	3.725	225.727	19.0	9.0	3.0
	M	0.274	2	0.137	8.303	19.0	9.0	3.0
	N	0.498	2	0.249	15.091	19.0	9.0	3.0
	e	0.033	2	0.016		19.0	9.0	3.0
Mean values of impact force (8#)	L	57.314	2	28.657	71.642	19.0	9.0	3.0
	M	1.207	2	0.604	1.509	19.0	9.0	3.0
	N	2.861	2	1.431	3.576	19.0	9.0	3.0
	e	0.800	2	0.400		19.0	9.0	3.0

2. As shown in statistical table of mean values of debris flow impact force, the mean values of impact force debris flow of the above eight key points have the largest values under the working condition of $L_3 M_1 N_3$.

References

Armanini A, Scotton P (1993) On the dynamic impact of a debris flow on structures. In: Proceeding of XXV congress of IAHR. Technical session B, Debris flows and landslides. [s.l.]: [s.n], 230-210

Bugnion L, McArdell BW, Bartelt P, Wendeler C (2012) Measurements of hills lope debris flow impact pressure on obstacles. Landslides 9(2):179–187

Chen HK, Tang HM, Chen YY (2007) Highway debris flow mechanics. Science Press, Beijing

Chen HK, Tang HM, Xian XF, Zhang YP (2010) Experimental model of debris flow impact features. J Chongqing Univ 33(5):114–119

Cui P, Zeng C, Lei Y (2015) Experimental analysis on the impact force of viscous debris flow. Earth Surface Process Landf 40:1644–1655

DeNatale JS, Iverson RM, Major J, LaHusen RG, Fiegel GL, Duffy JD (1999) Experimental testing of flexible barriers for containment of debris flows. US Geol Surv Open-File Rep 99–205, 3 p

He XY, Tang HM, Zhu XZ, Cheng HK (2013) Tests for impacting characteristics of debris flow slurry. J Vib Shock 32(24):127–134

He XY, Tang HM, Chen HK (2014a) Experimental study on impacting characteristic of debris flow considering different slurry viscosities, solid phase ratios and grain diameters. Chin J Geotech Eng 36(5):977–982

He XY, Chen HK, Tang HM, Zhu XZ (2014b) Experimental study on impacting characteristics of debris flow heads. J Chongqing Jiaotong Univ Nat Sci 33(1):85–89. doi:10.3969/j.issn.1674-0696.2014.01.19

Hu KH, Wei FQ, Hong Y, Li XY (2006) Field measurement of impact force of debris flow. Chin J Rock Mech Eng 25(1):2813–2819 **(In Chinese, with English abstract)**

Hu KH, Wei FQ, Li Y (2011) Real-time measurement and preliminary analysis of debris-flow impact force at Jiangjia Ravine, China. Earth Surf Process Landf 36(9):1268–1278. doi:10.1002/esp.2155

Hübl J, Suda J, Proske D, Kaitna R, Scheidl C (2009) Debris flow impact estimation. In: Proceedings, international symposium on water management and hydraulic engineering, Ohrid/Macedonia, pp 137–148

Iverson RM, Matthew L, Lahusen RG, Berti M (2010) The perfect debris flow? Aggregated results from 28 large-scale experiments. J Geophys Res Atmos 115(F3):438–454. doi:10.1029/2009JF001514

Ji LJ, Si YF, Liu HF, Song XL, Zhu W, Zhu AP (2014) Application of orthogonal experimental design in synthesis of mesoporous bioactive glass. Microporous Mesoporous Mater 184(1):122–126. doi:10.1016/j.micromeso.2013.10.007

Jia C, Zhang K, Zhang QY, Xu K (2014) Research on multi-factor optimization of underground laminated salt rock storage group based on orthogonal experimental design. Rock Soil Mech 35(6):1718–1726 **(In Chinese, with English abstract)**

Jiang TC (1985) Orthogonal Experimental Design. Shandong Technology Press, Jinan

Jiang ZX (2014) A Brief Guide to the Earthquake Landslide Treatment Engineering Design. Southwest Jiao Tong University Press, Chengdu

König U (2006) Real scale debris flow tests in the Schesatobel-valley. Master's thesis, University of Natural Resources and Life Sciences, Vienna, Austria

Liu LJ, Wei H (1997) Study of impact of debris flow. J Sichuan Univ Eng Sci Ed 1(2):99–102

Okuda S, Okunishi K (1980) Observation at kamikamihori valley of Mt. Yakedake. Excursion guide-book the third meeting of JGU commission on field experiments in geomorphology, disaster prevention research institute Kyoto unit, Japan. 1–139

Scheidl C, Chiari M, Kaitna R, Müllegger M, Krawtschuk A, Zimmermann T, Proske D (2013) Analyzing debris-flow impact models, based on a small scale modeling approach. Surv Geophys 34(1):121–140

Tang QY, Feng MG (2002) Practical statistical analysis and DPS data system. Science and Technology Press, Beijing

Tang JB, Hu KH, Zhou GD, Chen HY, Zhu XH, Ma C (2013) Debris flow impact pressure signal processing by the wavelet analysis. J Sichuan Univ Eng Sci Ed 45(1):8–13 **(In Chinese, with English abstract)**

Valentino R, Barla G, Montrasio L (2008) Experimental analysis and micromechanical modeling of dry granular flow and impacts in laboratory flume tests[J]. Rock Mech Rock Eng 41(1):153–177

Wei H (1996) Experimental study on impact force of debris flow heads. China Railw Sci 17(3):50–62 **(In Chinese, with English abstract)**

Wendeler C, Bugnion L (2012) Large scale field testing of hill slope debris flows resulting in the design of flexible protection barriers. In: Proceedings of 12th Interpraevent Grenoble/France

Wendeler C, Volkwein A, Roth A, Denk M, Wartmann S (2007) Field measurements used for numerical modeling of flexible debris flow barriers. The fourth international conference on debris-flow hazards mitigation: mechanics, prediction and assessment

Wu JS, Kang ZC, Tian LQ, Zhang SC (1990) Observation and research of Jiangjia Ravine in Yunnan. Science Press, Beijing, China

Yang HJ, Wei FQ, Hu KH, Chernomorets S, Hong Y, Li XY, Xie T (2011) Measuring the internal velocity of debris flows using impact pressure detecting in the flume experiment. J Mt Sci 8(2):109–116

Zeng C (2014) Vulnerability assessment of building to debris flow hazard. Graduate University of Chinese Academy of Sciences, Beijing

Zhang SC (1993) A comprehensive approach to the observation and prevention of debris flows in China. Nat Hazards 7(1):1–23

Zhang SC, Yuan JM (1985) Debris flow impact and its test. Lanzhou Inst Glaciol Cryopedology Chin Acad Sci 4:269–274